Original Article

CAMBRIDGE
UNIVERSITY PRESS

"Geochronology and geochemistry of pelitic granulite from the South Delhi Terrane of the Aravalli Delhi Mobile Belt, NW India: implications for petrogenesis and geodynamic model"

M. Kumar, D. Prakash [ID], C. K. Singh, S. Singh, R. K. Pandey, Pradip K. Singh and B. Mahanta

Centre of Advanced Study in Geology, Banaras Hindu University, Varanasi 221005, India

Abstract

An attempt has been made to illustrate the evolution of pelitic granulite from south of the Balaram-Abu road, which lies in the South Delhi Terrane (SDT) of the Aravalli-Delhi Mobile Belt (ADMB), using geochemistry and geochronology. The current work offers a plausible explanation for the protolith of pelitic granulite, nature of the sediments and its provenance. The elemental geochemistry of the pelitic granulites reveals that the protolith is an arkosic to shaley type. The rare earth elements pattern shows that there is a negative Eu anomaly and a small excess of LREE over HREE. This means that the source of sediments probably has the same elements as the upper crust. However, the amounts of Sr, Nd and Pb vary a lot, which shows that the sediments supplied from two different types of sources (felsic and mafic) in different proportions from a Proterozoic terrain. The monazite geochronology indicates that the metamorphic overprint occurred between 797 Ma and 906 Ma. Additionally, the ages correlate to the debris that was formed between the 1188 Ma and 1324 Ma from magmatic/sedimentary sources for pelitic granulite. The present research provides a more in-depth understanding of the evolutionary history of the pelitic granulite that comprises the SDT in the ADMB region during the Proterozoic era.

1. Introduction

Granulites have been discovered during a wide range of geological time, ranging from the Neoarchean all the way up to the Miocene, which is quite recent in geological terms and in a wide range of tectonic settings (Pownall *et al.* 2014). In the continental correlation of the supercontinent models, these rocks are considered as of great importance. In this context, the granulites that are located inside the South Delhi Terrane of the ADMB in the northwest region of India are quite significant.

There are three stratigraphic units of rocks that constitute the Aravalli mountains in northwest India: the Bhilwara terrane (Archaean), Aravalli supergroup (Palaeoproterozoic) and Delhi supergroup (Meso-Neoproterozoic). The Banded Gneissic Complex (BGC) is located in the Aravalli-Delhi Mobile Belt (ADMB), which is included in the Archean Bhilwara terrane (Fig. 1a, b). Both of these names refer to the basement of the ADMB (Heron, 1953; Ahmad and Mondal, 2016). Sandmata complex and Mangalwar complex can be located in Bhilwara terrane (Fig. 1b). The ancient granulites and charnockites that date back to 1725–1622 Ma were emplace within the Sandmata Complex during the Aravalli orogeny (Sarkar *et al.* 1989; Fareeduddin & Kroner, 1998; Roy *et al.* 2012). Kishangarh nepheline syenite intruded at 1490 ± 150 Ma, while South Delhi Terrane (SDT) granites were also intruded at 1012 ± 78 Ma (Crawford, 1970). Additionally, due to deformations that occurred millions of years ago in the Aravalli-Delhi mountain ranges, the Sandmata rocks that are found along the terrane boundary have been bent (Naha & Halyburton, 1974; Sen, 1980; Srivastava, 2001; Bhowmik *et al.* 2010; Singh *et al.* 2010, 2020; Roy *et al.* 2012, 2016; Tiwari & Biswal, 2019; Biswal *et al.* 2022; Tiwari *et al.* 2022). Therefore, the older ages of the Mangalwar and Sandmata complexes are reset to younger ages, particularly in the northern part of the Banas shear zone (Bhowmik & Dasgupta, 2012; Ahmad & Mondal, 2016; Kumar *et al.* 2019; D'Souza *et al.* 2021). It is generally agreed that the collision between the Bundelkhand craton and the Marwar craton was the primary driving force behind the orogeny that resulted in the development of the ADMB (Bhowmik *et al.* 2010; Singh *et al.* 2010, 2020; Tiwari & Biswal, 2019; Biswal *et al.* 2022; Tiwari *et al.* 2022).

The Diwani hills of SDT are situated in the Banaskantha district of Gujarat, which is a part of northwestern region of India. The granulites are exposed along the southern flank of
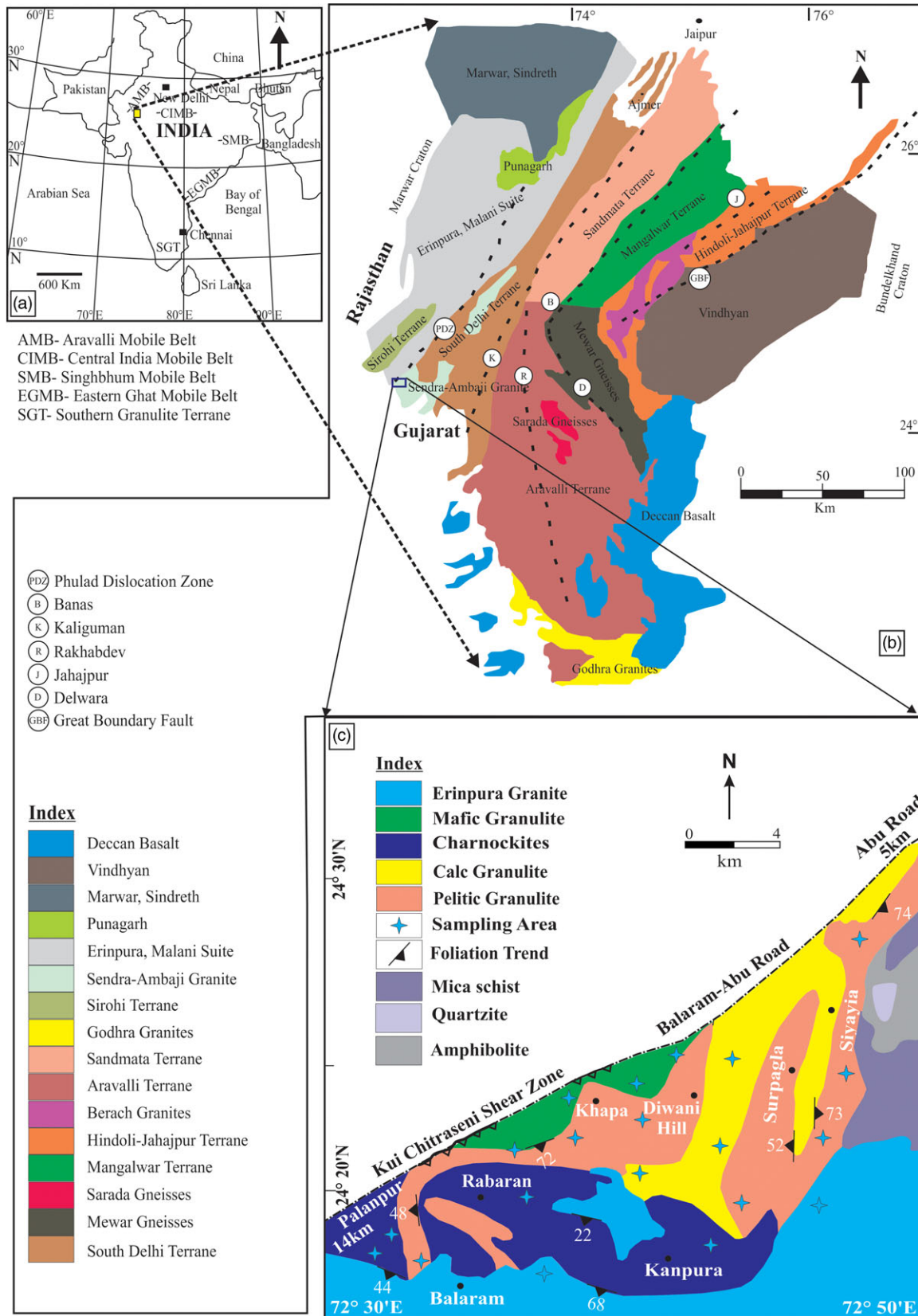
Figure 1. (Colour online) (a) Map of India showing different tectonic elements, modifed after Prakash *et al.* (2021). (b) Geological map of the Aravalli Mobile Belt (modified after Prakash *et al.* 2021). (c) Geological map of the study area showing sample location (map modified after Srikarni et. al, 2004; Singh *et al.* 2010; Prakash *et al.* 2021; Biswal *et al.* 2022).
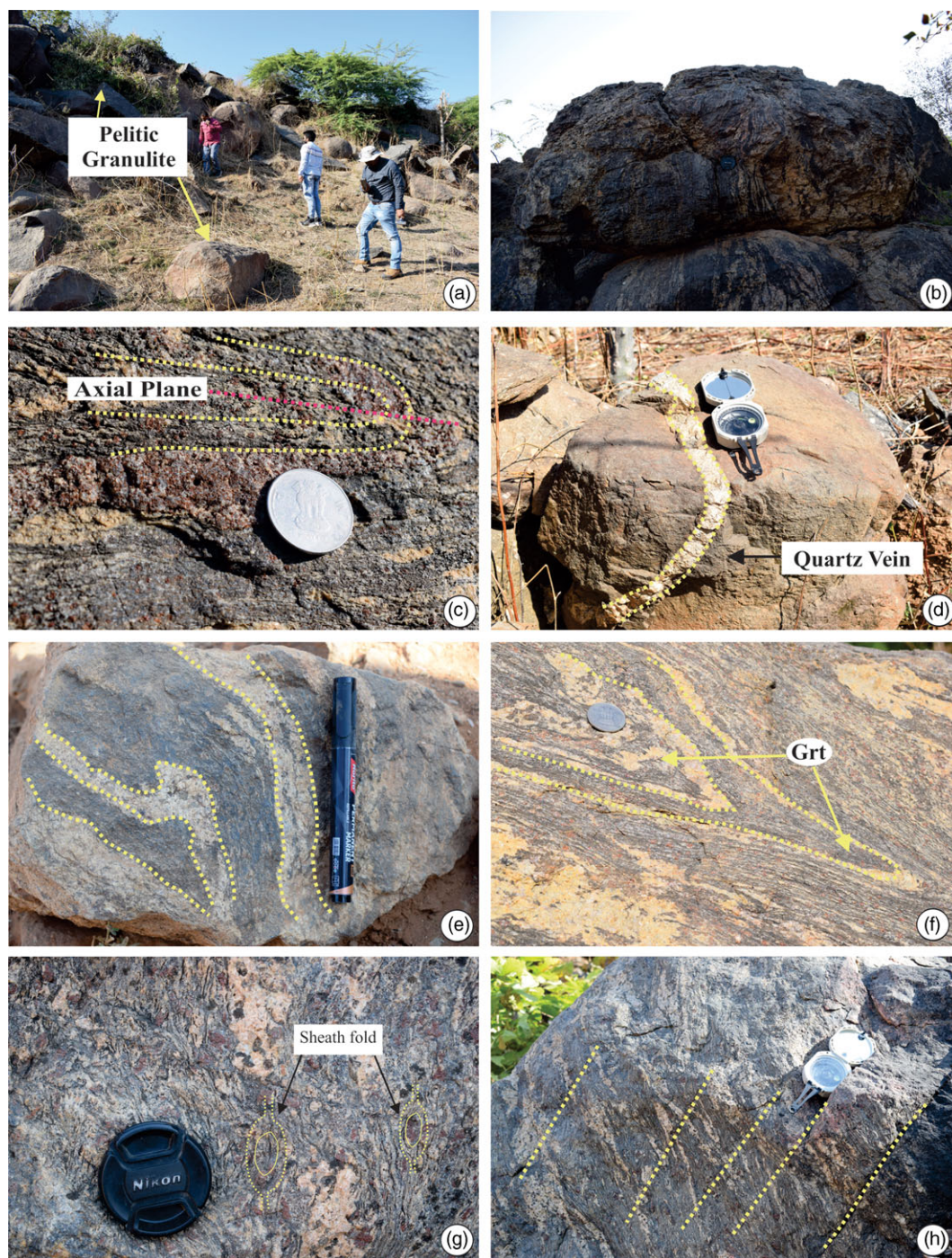
Figure 2. (Colour online) Field photographs of the principal rock types in the study area: (a) Study area shows well exposures of pelitic granulites near the village of Dhabeli. (b) Typical pelitic granulites with banding of colours. (c) Tight isoclinal fold is developed in response to severe compressional regeim near Chikanavos village. (d) Field photograph illustrating the evolution of a quartz vein near kanpura. (e) Pelitic granulites having alternating bands of luecocritic and melanocritic in near khapa village. (f) High concentration of garnet crystallization in the core of folding in the vicinity of Khapa village. (g) Core of sheath fold surrounded by folded migmatitic bands in pelitic granulites near Dhanpura village. (h) Joints with no obserable movement of blocks are also developed in pelitic granulites near Diwani hills.

Balaram-Abu road. These hills are composed of Precambrian crystalline rocks of both igneous and metamorphic in nature. In 1978, Desai and co-workers conducted the first investigation to demonstrate that granulite-facies rocks can be found in the region surrounding the Balaram-Abu Road. Near the Balaram-Abu Road, the rocks that occur frequently are charnockites, norites-metanorites, pelitic granulite, calc-granulite, mafic-granulite and granite (Desai *et al.* 1978). Pelitic granulite found in the region have a structure similar to gneiss and are composed of minerals that are organized into coarse bands of varying shades of light and dark colours having characteristic minerals such as spinel, cordierite, garnet, sillimanite, hypersthene, feldspar, quartz,
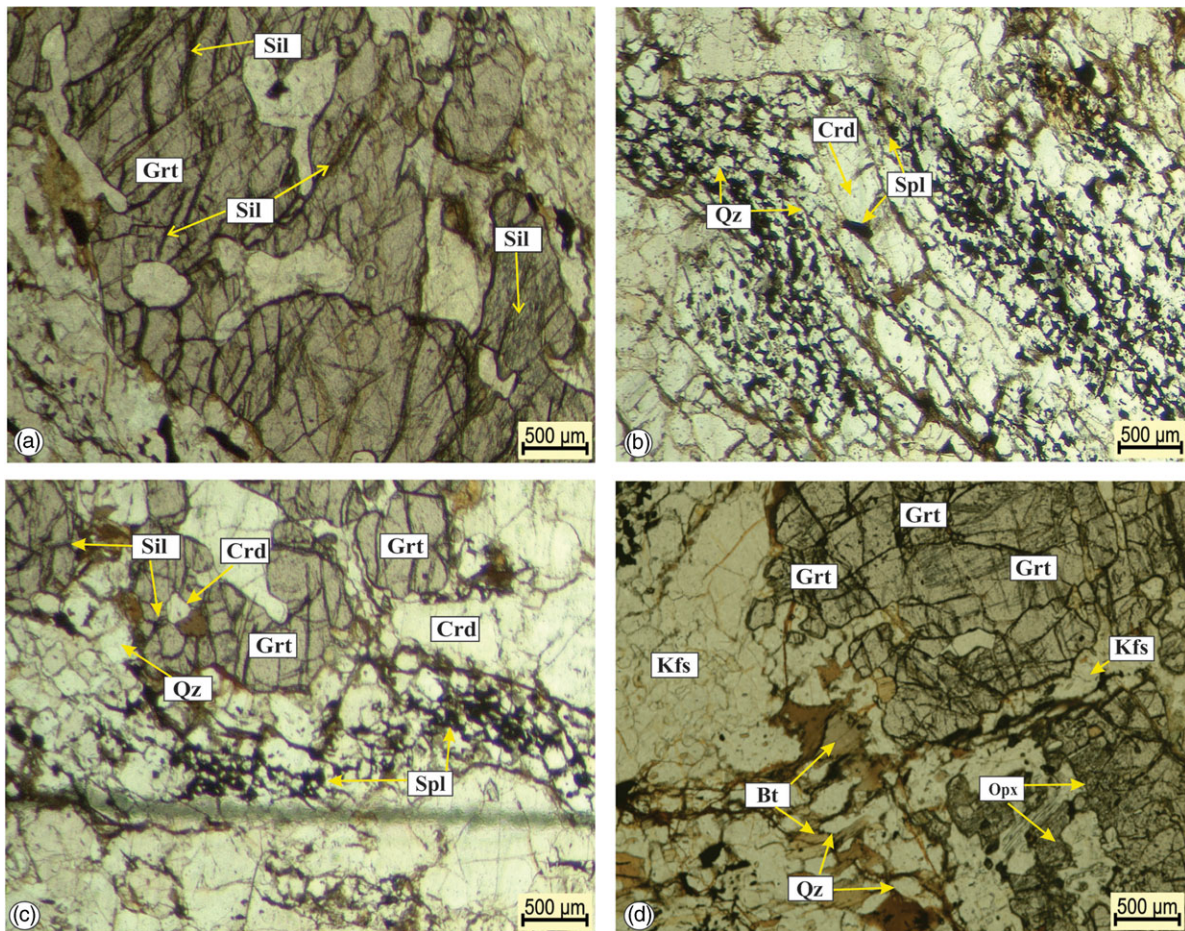
Figure 3. (Colour online) Photomicrographs of pelitic granulites. (a) Sillimanite occurs as inclusions within garnet. (b and c) Symplectitic intergrowth of spinel and cordierite. (d) Biotite quartz symplectites replaces garnet.

biotite and plagioclase. The lighter bands are composed of quartzo-feldspathic material, while the darker bands are predominantly composed of cordierite and contain reddish brown garnets scattered/dispersed throughout (Bhowmik *et al.* 2010; Singh *et al.* 2010, 2020; Tiwari & Biswal 2019; Prakash *et al.* 2021; Biswal *et al.* 2022; Tiwari *et al.* 2022).

The goal of this research is to investigate the geochemistry of major and trace elements in conjunction with the monazite geochronology of pelitic granulite from the SDT of ADMB, north Gujarat (Fig. 1c) to offer insight into the nature of protolith, tectonic context of the basin and provenance. In addition, we have provided a probable explanation for the evolution of pelitic granulite of the SDT.

2. Geological setting

The ADMB is a significant crustal morphotectonic unit, outstandingly exposed in the northwestern region of India. The study area is located in the southern portion of the Delhi supergroup, which is part of ADMB. This region consists of pelitic granulite, calc-granulite, mafic granulite and a variety of intrusives (Fig. 1). Pelitic granulite can be seen in the good exposures across the study area, such as close to the Dhabeli village (Fig. 2a, b). The area under investigation reveals numerous signatures of tectonic deformations, which may be correlated on the regional scale. Near the

village of Chikanavos, a tight isoclinal fold has developed as a response to the intense compressional regime (Fig. 2c). In some areas, the pelitic granulite grade into granite gneiss by passing through a zone of migmatites and display varying degrees of migmatization supposed to occur as a result of the gradual depletion of aluminosilicates and increase in quartzofeldspathic components. At certain locations, quartz veins display a discordant relationship with the country rocks (Fig. 2d). Strong evidences of the effects of regional metamorphism and partial melting are common in the study area in the form of migmatized pelitic granulite showing flow folding with leucocratic and melanocratic bandings near Khapa village (Fig. 2e). The presence of the high concentration of garnet crystallization in the core of the isoclinal folds has been observed, e.g., in the vicinity of Khapa village (Fig. 2f). Sheath folds, as evidence of intense deformation, have also been observed in the pelitic granulite (Fig. 2g). Parallel joints are also frequently common in the pelitic granulite throughout the study area (Fig. 2h). It has been observed that the gneissosity of pelitic granulite continues unabatedly into the granite gneiss via migmatites, becoming a part of the granite gneiss. In a manner that is consistent with the gneissosity of the granite gneiss, pelitic granulite-restites can be found embedded within the granite. This granite gneiss was equated with other granites of the SDT belt and identified as the Ambaji granite by the Geological Survey of India (1980). The Ambaji granite shows Rb-Sr isochron age of 850 Ma

Table 1a. Representative microprobe analyses and structural formulae of garnet and orthopyroxene

| Sample No. | D/93 | D/93 | D/93 | D/93 | D/93 | D/53 | D/53 | D/53 | D/93 | D/93 | D/93 | D/93 | D/93 | D/53 | D/53 | D/53 |
Mineral	Gt	Gt	Gt	Gt	Gt	Gt	Gt	Gt	Opx	Opx	Opx	Opx	Opx	Opx	Opx	Opx
SiO_2	37.58	39.73	38.89	37.13	36.13	35.85	37.02	36.51	50.40	49.29	48.35	49.17	48.39	50.29	47.39	50.29
TiO_2	0.48	0.49	0.01	0.47	0.10	0.02	0.00	0.01	0.00	0.44	0.17	0.27	0.34	0.00	0.34	0.00
Al_2O_3	17.24	21.67	21.38	22.10	21.85	20.16	19.38	19.98	3.84	4.23	4.99	4.41	4.72	4.13	4.72	4.13
Cr_2O_3	0.04	0.00	0.00	0.00	0.05	0.00	0.03	0.00	0.00	0.10	0.00	0.00	0.00	0.01	0.00	0.01
FeO	36.17	31.61	32.99	34.56	37.59	37.43	36.87	36.22	28.06	28.31	29.10	29.22	29.14	29.00	29.14	27.80
MnO	1.40	1.14	1.57	1.47	1.28	1.21	1.19	2.12	0.00	0.00	0.00	0.00	0.00	0.02	0.00	0.02
MgO	2.34	2.07	2.07	1.88	1.85	2.65	2.53	3.15	16.86	16.83	16.22	16.20	16.70	16.37	16.20	17.37
CaO	2.91	2.24	2.46	1.23	1.23	1.11	1.05	0.96	0.32	0.35	0.23	0.42	0.24	0.09	0.24	0.09
Na_2O	0.00	0.28	0.23	0.23	0.00	0.00	0.00	0.00	0.00	0.00	0.00	0.00	0.00	0.00	0.00	0.00
K_2O	0.01	0.00	0.00	0.00	0.01	0.00	0.00	0.01	0.00	0.00	0.00	0.00	0.00	0.00	0.00	0.00
Total	98.26	99.24	99.66	99.07	100.09	98.43	98.07	98.97	99.48	99.55	99.06	99.69	99.35	99.91	98.03	99.71
O	12	12	12	12	12	12	12	12	6	6	6	6	6	6	6	6
Si	3.121	3.143	3.101	2.999	2.935	2.970	3.062	2.997	1.932	1.896	1.877	1.896	1.871	1.926	1.866	1.920
Ti	0.030	0.029	0.001	0.029	0.006	0.001	0.000	0.001	0.000	0.013	0.005	0.008	0.010	0.000	0.010	0.000
Al	1.687	2.021	2.009	2.105	2.093	1.969	1.890	1.934	0.173	0.192	0.228	0.200	0.215	0.186	0.219	0.186
Cr	0.003	0.000	0.000	0.000	0.003	0.000	0.002	0.000	0.000	0.003	0.000	0.000	0.000	0.000	0.000	0.000
Fe^{2+}	2.352	2.092	2.200	2.335	2.554	2.534	2.504	2.418	0.881	0.905	0.945	0.938	0.942	0.909	0.959	0.874
Fe^{3+}	0.160	0.000	0.000	0.000	0.000	0.060	0.046	0.069	0.019	0.006	0.000	0.004	0.000	0.019	0.000	0.013
Mn	0.098	0.076	0.106	0.101	0.088	0.085	0.084	0.147	0.000	0.000	0.000	0.000	0.000	0.001	0.000	0.001
Mg	0.290	0.244	0.246	0.226	0.224	0.327	0.311	0.385	0.936	0.965	0.939	0.931	0.962	0.934	0.950	0.988
Ca	0.259	0.190	0.210	0.106	0.107	0.098	0.093	0.084	0.013	0.014	0.010	0.017	0.010	0.004	0.010	0.004
Na	0.000	0.044	0.036	0.036	0.000	0.000	0.000	0.000	0.000	0.000	0.000	0.000	0.000	0.000	0.000	0.000
K	0.001	0.000	0.000	0.000	0.001	0.000	0.000	0.001	0.000	0.000	0.000	0.000	0.000	0.000	0.000	0.000
X_{Mg}	0.103	0.104	0.100	0.088	0.081	0.112	0.109	0.134	0.522	0.516	0.498	0.498	0.505	0.507	0.498	0.531
$X_{Mg} = Mg/(Mg + Fe^{2+})$																
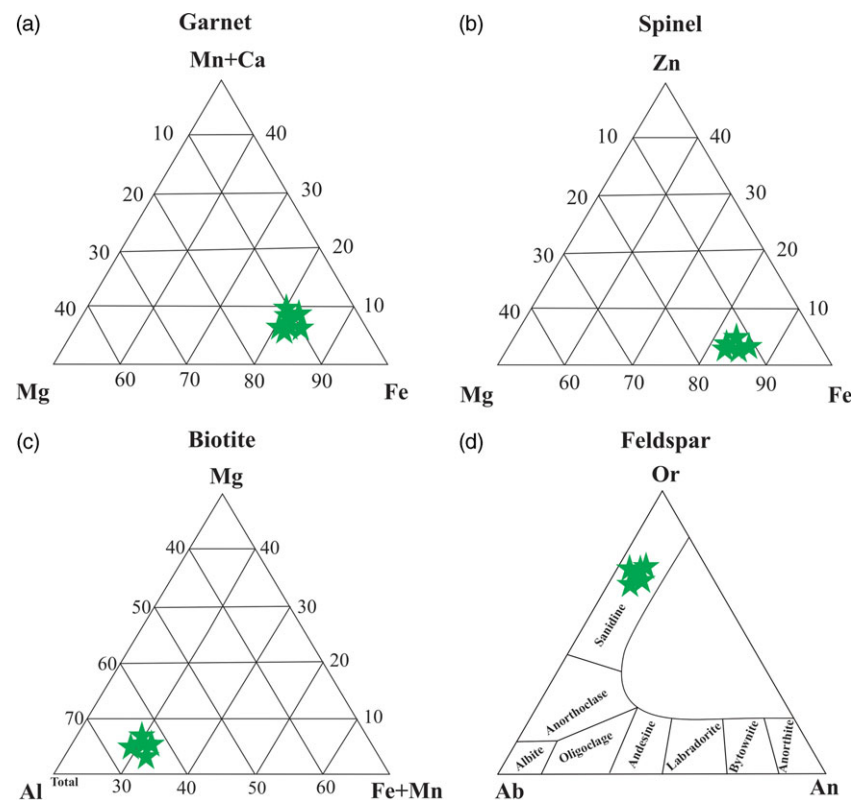
Figure 4. (Colour online) (a) Triangular plot of garnet showing Fe-rich composition. (b) Triangular plot of spinel showing Fe-rich composition. (c) Triangular plot of biotite showing relatively high Fe + Mn and Al content as compared to Mg content. (d) Triangular plot of feldspar showing higher concentration of sanidine and oligoclase composition.

(Choudhary *et al.* 1984). Volcanic rocks interlayered with metasediments are known as meta-rhyolite and meta-basalt, which most likely originated from syn-sedimentary volcanism. The metasediments and granite gneiss have been disrupted by the intrusion of a gabbro-norite-basic granulite suite, which the Geological Survey of India in 1980 referred to as the Phulad Ophiolite suite. The emplacement of gabbro-norite-basic granulite intrusives is geographically and temporally connected to the granulite facies metamorphism that occurred in the region. Thus, the amphibolite and granulite facies rocks, as well as certain obducted ophiolites, basement gneisses and blueschists, make up the SDT (Volpe & Macdougall, 1990; Tobisch *et al.* 1994; Biswal et al; Srikarni *et al.* 2004; Mukhopadhyay *et al.* 2010; Bhowmik *et al.* 2018). The age of the South Delhi orogeny can be restricted between 1.7 and 0.8 Ga ago experiencing multiple folding events and high-grade metamorphism (Choudhary *et al.* 1984; Volpe & Macdougall, 1990; Tobisch *et al.* 1994; Deb & Thorpe, 2001; Deb *et al.* 2001; Pandit *et al.* 2003). It is believed that basin was likely closed due to subduction along the Kaliguman shear zone, which serves as a contact/suture between the Delhi Terrane and the Aravalli Terrane (Sugden *et al.* 1990; Biswal *et al.* 1998a).

In terms of brittle, ductile and brittle-ductile deformations, the study area is characterized by the presence of a great number of deformed zones that have given rise to shears and faults at regional scale, including the Kui-Chitraseni shear zone, the Surpagla shear zone and the Deldar shear zone. The Kui-Chitraseni shear zone is the extension of the Phulad Dislocation Zone (PDZ), and it stands out as an enormous fault striking NNE-SSW. It runs roughly parallel to the Banas river, and it is considered to preserve evidence of reactivation of the fault (Biswal *et al.* 2004; Sarkar & Biswal, 2005; Anbazhagan *et al.* 2006; Bhowmik *et al.* 2010; Singh *et al.* 2010, 2020; Tiwari & Biswal, 2019; Tiwari *et al.* 2022; Biswal *et al.* 2022). Exhumation of the granulites terrene was caused by

thrusting and obduction that occurred between the terrane borders of the Surpagla and Kui-Chitraseni faults.

3. Textural relationships

The detailed petrographic study revealed the presence of diverse mineral assemblages. Garnet, spinel, K-feldspar, biotite, quartz, plagioclase, orthopyroxene and cordierite are the main components of the pelitic granulite. In addition to the minerals mentioned above, trace amounts of magnetite, ilmenite, rutile, zircon, graphite and apatite are also present. Prograde stage of metamorphism is marked by the presence of sillimanite as inclusion within the garnet (Fig. 3a). Cordierite most ften occurs as larger grain and is frequently found in close association with spinel (Fig. 3b). Cordierite grains are found to be very close to spinel and quartz. The probable reaction for such texture is combination of spinel and quartz give rise to cordierite. The subsequent stage is characterized by the resorption of garnet through the development of spectacular symplectites (a linear clump of spinel with quartz and cordierite, Fig. 3c) along with cordierite forming reaction, diagnostic of decompressional regime. During the late stage, biotite-quartz symplectite replaced with the garnet blast (Fig. 3d).

4. Mineral chemistry

The Electron Probe Micro Analyzer (EPMA) CAMECA SXFive instrument equipped with SXFive software at the DST-SERB National Facility, Department of Geology (Center of Advanced Study), Institute of Science, Banaras Hindu University has been used to detect the mineral compositions of representative rock types from the Diwani hills for the purpose of mineral chemistry. In order to accomplish this goal, in the beginning, the polished thin sections were given a layer of carbon that was

Table 1b. Representative microprobe analyses and structural formulae of spinel, biotite and cordierite

Sample No.	D/93	D/93	D/93	D/53	D/53	D/93	D/93	D/53	D/53	D/53	D/93	D/93	D/93	D/53	D/53
Mineral	Spl	Spl	Spl	Spl	Spl	Bt	Bt	Bt	Bt	Bt	Crd	Crd	Crd	Crd	Crd
SiO_2	0.03	0.04	0.03	0.01	0.01	35.10	32.48	39.45	34.82	34.70	48.05	46.22	45.02	44.40	43.37
TiO_2	0.05	0.02	0.03	0.02	0.05	2.46	3.61	2.46	2.46	3.07	0.00	0.03	0.00	0.00	0.00
Al_2O_3	53.65	56.07	56.19	56.56	55.16	19.06	22.98	19.52	17.26	18.47	38.44	36.42	37.96	38.31	39.88
Cr_2O_3	0.21	0.21	0.32	0.22	0.12	0.00	0.00	0.00	0.00	0.00	0.00	0.00	0.00	0.00	0.09
FeO	40.99	38.72	39.27	39.33	41.67	19.77	18.70	21.66	28.18	24.40	6.19	14.82	11.49	10.82	8.56
MnO	0.17	0.17	0.18	0.08	0.08	0.00	0.01	0.00	0.00	0.00	0.12	0.07	1.87	1.35	1.03
MgO	2.95	1.68	2.31	1.77	1.65	2.85	8.92	5.94	11.80	15.82	5.82	2.00	2.81	4.02	6.56
CaO	0.04	0.02	0.00	0.02	0.00	0.05	0.05	0.05	0.05	0.02	0.00	0.03	0.03	0.03	0.03
Na_2O	0.05	0.02	0.03	0.02	0.02	0.02	0.04	0.09	0.00	0.02	0.00	0.03	0.00	0.00	0.00
K_2O	0.01	0.00	0.00	0.02	0.00	18.19	12.00	10.81	4.02	3.15	0.00	0.02	0.01	0.02	0.00
ZnO	0.24	0.32	0.35	0.96	0.79	0.00	0.00	0.00	0.00	0.00	0.00	0.00	0.00	0.00	0.00
Total	98.38	97.27	98.70	99.03	99.55	97.49	98.80	99.97	98.59	99.65	99.62	98.80	98.94	99.96	98.18
O	4	4	4	4	4	22	22	22	22	22	18	18	18	18	18
Si	0.001	0.001	0.001	0.000	0.000	5.514	4.837	5.744	5.190	5.000	4.858	4.826	4.696	4.626	4.456
Ti	0.001	0.000	0.001	0.000	0.001	0.290	0.404	0.269	0.275	0.333	0.000	0.002	0.000	0.000	0.000
Al	1.883	1.961	1.940	1.951	1.916	3.529	4.034	3.349	3.031	3.137	4.582	4.482	4.667	4.705	4.829
Cr	0.005	0.005	0.007	0.005	0.003	0.000	0.000	0.000	0.000	0.000	0.000	0.000	0.000	0.000	0.008
Fe^{2+}	0.911	0.929	0.911	0.919	0.947	2.597	2.329	2.637	3.511	2.939	0.523	1.294	1.002	0.943	0.735
Fe^{3+}	0.110	0.032	0.051	0.043	0.080	0.000	0.000	0.000	0.000	0.000	0.000	0.000	0.000	0.000	0.000
Mn	0.004	0.004	0.005	0.002	0.002	0.000	0.002	0.000	0.000	0.000	0.010	0.006	0.165	0.119	0.090
Mg	0.131	0.074	0.101	0.077	0.073	0.667	1.981	1.289	2.621	3.397	0.877	0.312	0.437	0.625	1.004
Ca	0.001	0.001	0.000	0.001	0.000	0.009	0.008	0.008	0.008	0.003	0.000	0.003	0.003	0.003	0.003
Na	0.003	0.001	0.002	0.001	0.001	0.006	0.013	0.025	0.000	0.004	0.000	0.007	0.000	0.000	0.000
K	0.001	0.000	0.000	0.001	0.000	3.644	2.281	2.008	0.765	0.579	0.000	0.003	0.001	0.003	0.000
Zn	0.005	0.007	0.008	0.021	0.017	0.000	0.000	0.000	0.000	0.000	0.000	0.000	0.000	0.000	0.000
X_{Mg}	0.114	0.072	0.095	0.074	0.066	0.204	0.460	0.328	0.427	0.536	0.626	0.194	0.304	0.398	0.577

$X_{Mg} = Mg/(Mg + Fe^{2+})$

Table 1c. Representative microprobe analyses and structural formulae of K-feldspar, sillimanite and ilmenite

| Sample No.	D/93	D/93	D/53	D/53	D/53	D/93	D/93	D/53	D/53	D/53	D/93	D/93	D/53	D/53	D/53
Mineral	Kfs	Kfs	Kfs	Kfs	Kfs	Sil	Sil	Sil	Sil	Sil	Ilm	Ilm	Ilm	Ilm	Ilm
SiO_2	63.96	64.26	64.58	63.96	63.48	35.96	34.48	36.25	32.58	36.96	0.00	0.00	0.00	0.00	0.00
TiO_2	0.12	0.00	0.04	0.04	0.03	0.04	0.03	0.00	0.04	0.04	51.45	52.72	53.95	52.93	51.69
Al_2O_3	18.11	18.31	18.35	18.28	18.08	62.96	64.48	64.24	65.58	60.96	0.00	0.00	0.00	0.00	0.00
Cr_2O_3	0.06	0.00	0.04	0.00	0.03	0.00	0.03	0.00	0.04	0.00	0.00	0.00	0.00	0.00	0.00
FeO	0.05	0.25	0.08	0.00	0.00	0.00	0.00	0.03	0.08	0.00	47.21	45.72	44.21	45.09	45.91
MnO	0.00	0.02	0.00	0.00	0.00	0.00	0.00	0.00	0.00	0.00	0.36	0.47	0.33	0.29	0.51
MgO	0.00	0.00	0.02	0.02	0.01	0.00	0.01	0.00	0.02	0.00	0.06	0.06	0.04	0.03	0.00
CaO	0.00	0.01	0.09	0.06	0.07	0.06	0.07	0.01	0.09	0.06	0.04	0.02	0.04	0.06	0.09
Na_2O	0.88	1.85	1.19	1.25	1.76	0.00	0.02	0.02	0.00	0.00	0.00	0.00	0.00	0.00	0.00
K_2O	14.50	12.99	14.19	14.33	13.32	0.00	0.00	0.00	0.00	0.00	0.00	0.00	0.00	0.00	0.00
Total	97.68	97.66	98.58	97.92	96.79	99.02	99.13	100.55	98.42	98.02	99.12	98.99	98.57	98.41	98.20
O	8	8	8	8	8	5	5	5	5	5	6	6	6	6	6
Si	3.004	3.003	3.002	2.997	2.999	0.980	0.941	0.973	0.897	1.016	0.00	0.00	0.00	0.00	0.00
Ti	0.004	0.000	0.001	0.001	0.001	0.001	0.001	0.000	0.001	0.001	3.959	4.031	4.109	4.059	3.999
Al	1.002	1.008	1.005	1.010	1.007	2.024	2.075	2.034	2.130	1.976	0.000	0.000	0.000	0.000	0.000
Cr	0.002	0.000	0.002	0.000	0.001	0.000	0.001	0.000	0.001	0.000	0.000	0.000	0.000	0.000	0.000
Fe	0.002	0.010	0.003	0.000	0.000	0.000	0.000	0.001	0.002	0.000	2.019	1.943	1.872	1.922	1.974
Mn	0.000	0.000	0.000	0.000	0.000	0.000	0.000	0.000	0.000	0.000	0.016	0.020	0.014	0.013	0.022
Mg	0.000	0.000	0.001	0.000	0.001	0.000	0.000	0.000	0.001	0.000	0.004	0.005	0.003	0.002	0.000
Ca	0.000	0.000	0.005	0.003	0.004	0.002	0.002	0.000	0.003	0.002	0.002	0.001	0.002	0.003	0.005
Na	0.080	0.168	0.107	0.114	0.162	0.000	0.001	0.001	0.000	0.000	0.000	0.000	0.000	0.000	0.000
K	0.869	0.774	0.842	0.857	0.803	0.000	0.000	0.000	0.000	0.000	0.000	0.000	0.000	0.000	0.000
X_k	0.915	0.822	0.883	0.880	0.829	0.000	0.000	0.000	0.000	0.000	0.000	0.000	0.000	0.000	0.000
$X_k = K/(K + Na + Ca)$															

Table 2a. Chemical composition of pelitic granulite. Major oxides (%) and rare earth elements (PPM)

Sample No.	D/1	D/15	D/17	D/26	D/47	D/48	D/53	D/68	D/69	D/72	D/73	D/93
SiO_2	63.17	63.16	63.78	82.47	68.45	64.98	69.80	69.81	59.46	72.27	76.43	71.25
Al_2O_3	16.84	18.19	17.07	6.89	15.13	17.73	13.76	13.90	15.32	14.48	12.58	14.38
Fe_2O_3	7.47	9.62	9.20	5.00	8.85	6.91	8.86	8.24	8.70	3.29	4.62	3.97
MgO	2.58	2.29	2.29	1.34	2.24	1.87	2.18	2.11	1.85	1.53	1.50	2.63
CaO	0.18	0.21	0.18	0.17	0.20	0.22	0.27	0.26	1.15	1.34	0.52	1.35
Na_2O	0.39	0.48	0.36	0.18	0.37	0.65	0.32	0.35	1.32	2.81	2.13	2.59
K_2O	3.51	3.73	3.82	1.83	2.68	5.53	2.76	3.15	3.66	4.68	4.78	4.42
TiO_2	1.19	1.08	1.12	0.79	1.03	0.99	1.06	1.05	1.30	0.25	0.62	0.27
P_2O_5	0.05	0.04	0.05	0.03	0.04	0.08	0.05	0.05	0.40	0.11	0.03	0.13
MnO	0.15	0.12	0.14	0.05	0.11	0.08	0.12	0.10	0.13	0.02	0.05	0.05
Cr_2O_3	0.02	0.02	0.02	0.01	0.02	0.02	0.02	0.02	0.01	0.00	0.00	0.00
LOI	1.20	0.90	1.00	1.60	0.70	0.70	0.60	0.80	0.90	1.10	0.80	0.90
Total	**99.89**	**99.90**	**99.92**	**99.95**	**99.91**	**99.92**	**99.92**	**99.92**	**99.93**	**99.98**	**100.00**	**99.98**
La	48.70	52.70	36.80	44.60	47.20	47.20	49.90	42.90	37.30	46.00	10.80	56.40
Ce	107.03	114.37	82.67	97.47	98.92	100.47	104.70	95.27	87.80	89.71	27.52	108.11
Pr	12.80	13.10	9.60	10.80	11.50	11.40	12.30	11.20	11.50	9.40	3.20	11.90
Nd	45.50	48.00	35.90	39.00	41.60	41.50	44.10	40.10	46.90	31.40	10.80	39.10
Sm	8.90	9.20	7.10	7.80	8.00	8.00	8.40	7.80	10.70	5.30	2.90	6.70
Eu	1.00	1.10	1.00	0.60	1.10	2.10	1.00	1.00	2.50	0.90	<0.1	0.90
Gd	7.50	7.70	6.50	6.50	7.00	6.50	7.30	6.60	10.60	3.80	3.60	5.20
Tb	1.10	1.10	1.10	0.90	1.10	0.90	1.10	1.00	1.60	0.40	1.00	0.70
Dy	6.50	6.80	8.50	4.90	7.20	4.70	7.30	5.90	9.70	2.00	10.10	4.40
Ho	1.30	1.40	2.00	0.90	1.60	0.90	1.60	1.20	1.90	0.30	2.70	0.90
Er	4.00	4.20	6.60	2.60	5.20	2.40	5.10	3.80	5.40	0.80	9.70	2.50
Tm	0.60	0.60	1.00	0.40	0.80	0.30	0.80	0.60	0.70	0.10	1.60	0.30
Yb	3.90	4.00	6.40	2.40	5.10	2.10	5.00	3.60	4.60	0.60	10.30	1.90
Lu	0.60	0.60	0.90	0.40	0.80	0.30	0.70	0.50	0.70	<0.1	1.40	0.30
Y	41.00	39.00	59.00	27.00	47.00	24.00	45.00	39.00	53.00	10.00	101.00	25.00
Sc	22.40	21.90	26.50	9.80	23.10	13.80	20.60	17.50	18.50	3.40	3.80	8.80

20 nanometers thick so that electron probe microanalyses could be performed on them with the assistance of the LEICA-EM ACE200 apparatus.

The microprobe data and structural formulations for Garnet based on 12 oxygen a.p.f.u. from pelitic granulite are shown in Table 1a. The X_{Mg} content of the garnet ranges from 0.081 to 0.134. The analysed garnets were plotted in a ternary diagram consisting of Fe, Mg and (Ca + Mn), which reveals the concentration in the almandine and pyrope zones (Fig. 4a). The microprobe data for Orthopyroxenes are presented in Table 1a, together with the structural formulations based on 6 oxygen a.p.f.u. The Al_2O_3 ranges between 3.84 and 4.99, whereas MgO reaches upto 17.37 weight percent. X_{Mg} ranges from 0.498 to 0.531. The examined spinel is a solid solution of hercynite mostly, which is iron rich. The hercynite ($Fe_2Al_2O_4$) that makes up the majority of the spinel in the pelitic granulite has X_{Mg} values that range between 0.066 and

0.144. Al_2O_3 is found in spinel in high concentrations (up to 56.56 weight %), as is FeO (41.67 weight %) (Table 1b). Hercynite ($Fe_2Al_2O_4$) makes up the majority of spinel in the rocks that were examined, and there is only a trace amount of zinc oxide (less than 0.96 weight %). When plotted in a ternary diagram consisting of $ZnAl_2O_3$ (gahnite), $MgAl_2O_4$ (spinel) and $FeAl_2O_4$ (hercynite), the composition of spinel is found to be rich in hercynite (Fig. 4b). The structural formulations (based on 22 oxygen a.p.f.u.) and microprobe analyses of Biotite show a wide range of X_{Mg} values (Table 1b), ranging from 0.204 to 0.536. The compositions of biotite are plotted in Mg – Al – (Fe + Mn) triangular diagram (Fig. 4c). Appreciable amounts of TiO_2 are present with TiO_2 concentrations ranging between 2.46 and 3.61 wt %. The analyses of Cordierite show low anhydrous sums of oxides, between 98 and 99 % (Table 1b). This indicates the presence of around 1–2 weight % of a hydrous component (H_2O and/or CO_2) that is present inside
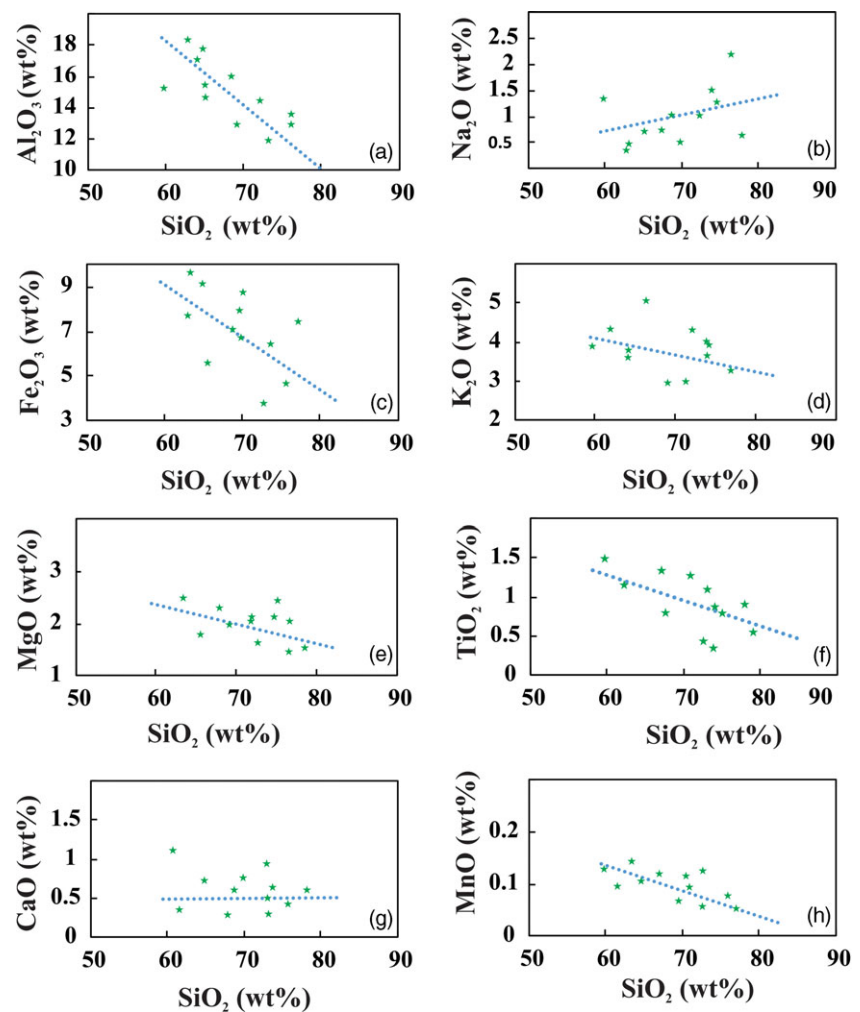
Figure 5. (Colour online) Harker variation graphs, showing the relation of Al_2O_3, Fe_2O_3, K_2O, TiO_2, MgO, MnO, Na_2O and CaO with increase of SiO_2.

structural channels. The amount of X_{Mg} that is included in the cordierite ranges between 0.194 and 0.626. The orthoclase-content X_{Or} [K/(K + Na + Ca)] in K-feldspar ranges between 0.822 and 0.883 (Fig. 4d). The analyzed composition of sillimanite closely resembles its ideal composition. Al_2O_3 and SiO_2 are present as major oxides in the sillimanite structure. The Si-content ranges between 1.437 and 1.626 pfu, whereas Al-content varies from 3.161 to 3.409 pfu. Microprobe analyses of ilmenite, on the whole, reveal low anhydrous sums of oxides, which translates to a percentage range of 98.20–99.12% (Table 1c). MnO, MgO and CaO are present at trace levels while TiO_2 ranges between 51.45 wt % and 53.95 wt % in the analysed ilmenite.

5. Geochemistry of whole-rock samples

5.a. Analytical method

Whole-rock geochemical data were carried out at Bureau Veritas Commodities Ltd, Canada. (see for details: https://commodities. bureauveritas.com/metals minerals/exploration-and-mining/geo-analytical-services). Cautiously fresh and unfractured samples have been selected for this analysis to avoid any contamination. Lithium metaborate and lithium tetraborate fusion analysis, also known as $LiBO_2$/$Li_2B_4O_7$ fusion analysis, was used to determine the major element concentrations of granulites. This was then followed by ICP-ES procedures. The 4 Acid digestions Ultratrace ICP-MS method was used to test trace elements, which are typically less than 0.1% by weight. Mixtures of entire rock powders (0.5 g) and $Li_2B_4O_7$ + $LiBO_2$ (4.5 g) were taken into glass discs for the purpose of conducting major element analysis. The discs were then subjected to X-ray fluorescence spectroscopy. The chemical assay method was utilized to determine the FeO, while the wet chemical method was utilized to determine the loss on ignition (LOI).

5.b. Major element characteristics

Twelve samples were selected in order to represent the pelitic granulite in the study area. Geochemical data of major and trace element are presented in Table 2a. Pelitic granulite show variable composition of silica (ranging from 59.46 to 82.47wt %) and low content of CaO (0.17 to 1.35 wt %), MgO (1.34 to 2.63 wt %), TiO_2 (0.25 to 1.30 wt %) and MnO (0.02 to 0.15 wt %). The total alkali concentration varies from 2.30 to 6.15 wt %, whereas the Al_2O_3 content fluctuates from 6.89 to 18.19 wt %. The range of K_2O is greater (1.83 and 5.53 wt %) as compared to Na_2O (0.18 and 2.81 wt %). The pelitic granulite have a K_2O/Na_2O ratio that ranges from 0.33 to 3.00, indicating that they contain a significant

Table 2b. Chemical composition of pelitic granulite. Major elements (%) and trace elements (PPM)

Sample No.	D/1	D/15	D/17	D/26	D/47	D/48	D/53	D/68	D/69	D/72	D/73	D/93
Fe	6.93	6.63	6.92	3.62	6.23	4.81	6.12	5.61	5.92	1.53	1.09	2.79
Ca	0.12	0.15	0.12	0.13	0.14	0.15	0.19	0.18	3.17	0.91	0.35	0.94
P	0.03	0.02	0.02	0.01	0.02	0.04	0.03	0.03	0.18	0.05	0.01	0.06
Ti	0.69	0.65	0.66	0.45	0.60	0.59	0.63	0.64	0.93	0.13	0.01	0.16
Al	8.38	8.66	7.73	3.42	7.70	8.64	7.20	6.84	7.96	7.42	5.88	7.54
Na	0.31	0.39	0.30	0.16	0.31	0.52	0.26	0.27	2.63	2.14	2.34	2.00
Mg	1.50	1.34	1.29	0.83	1.33	1.11	1.29	1.18	1.09	0.31	0.03	0.38
K	2.88	3.18	3.20	1.15	2.31	4.70	2.33	2.65	3.12	3.82	3.96	3.68
Cu	47.90	5.90	4.70	56.90	18.60	11.10	14.40	19.00	12.80	13.50	3.10	20.20
Co	30.90	25.40	25.80	16.20	23.10	19.70	22.20	22.30	17.70	3.70	0.40	5.50
Ni	85.00	57.00	60.00	47.00	49.00	50.00	46.00	56.00	20.00	19.00	21.00	19.00
Zn	140.7	125.7	125.9	82.1	120.6	88.9	107.7	105.0	100.2	38.9	27.8	44.1
Rb	158.6	175.9	188.3	93.9	120.5	252.4	148.6	155.1	130.1	191.3	365.9	185.2
Li	28.90	18.20	17.40	16.10	17.90	8.10	11.30	10.50	25.10	24.00	38.40	24.50
Cr	119.0	109.0	98.0	55.0	95.0	82.0	101.0	97.0	25.0	6.0	3.0	11.0
Hf	1.50	1.37	1.11	2.23	1.52	1.14	1.65	1.61	2.05	2.21	2.76	2.71
Ta	0.90	0.90	1.00	0.80	1.00	1.00	0.90	0.90	1.40	0.50	0.60	0.70
Nb	18.54	18.63	19.62	16.36	17.07	16.71	18.56	18.01	22.45	6.67	2.41	8.42
Th	25.60	27.40	20.90	23.00	23.00	23.20	24.20	22.80	11.00	31.20	5.30	37.50
Sr	59.00	55.00	51.00	26.00	46.00	98.00	42.00	49.00	195.00	106.00	6.00	101.00
Mo	0.29	0.30	0.24	0.31	0.39	0.36	0.32	0.36	1.03	0.86	0.15	1.37
Pb	22.31	20.34	23.55	10.39	17.40	31.30	13.85	15.21	22.99	37.89	34.06	38.98
Mn	1171.0	919.0	1124.0	381.0	917.0	597.0	1013.0	774.0	1021.0	133.0	387.0	372.0
V	160.0	145.0	119.0	70.0	113.0	117.0	118.0	115.0	95.0	14.0	30.0	20.0
Ba	471.0	445.0	485.0	189.0	412.0	842.0	329.0	365.0	611.0	497.0	6.0	505.0
Zr	55.30	50.30	40.60	80.40	56.30	41.40	62.30	60.80	82.90	76.40	63.30	92.90
Sn	0.20	0.30	0.20	0.10	0.50	0.30	0.20	0.30	3.50	2.30	9.90	2.20
Y	34.00	36.30	48.10	24.60	42.40	22.10	43.10	33.00	50.20	8.90	74.00	24.70
Cs	2.40	2.50	2.30	1.50	2.70	2.30	2.20	2.00	3.70	4.30	12.80	3.70
Ga	24.51	26.81	25.17	11.81	21.95	22.19	21.29	20.96	25.45	15.89	19.98	15.61
As	1.60	0.90	<0.2	0.30	0.30	0.20	0.30	0.30	2.00	2.10	1.90	1.70
U	2.20	2.20	2.20	2.10	2.40	2.30	2.30	2.20	2.30	1.60	3.10	1.90

amount of K-feldspar. The geochemistry of the pelitic granulite in the area that was investigated provides some support for the hypothesis that the protolith has an arkosic to shaley character. Al_2O_3, Fe_2O_3, K_2O, TiO_2, MgO and MnO all show a systematic reduction with increasing SiO_2 in the Harker variation graphs (Fig. 5), but Na_2O shows a systematic increase with rising SiO_2. However, as shown in Fig. 5, there is no correlation between SiO_2 and CaO.

5.c. Trace element characteristics

Geochemical data of trace elements and rare earth elements (REE) are presented in Table 2b. Tables 2 and 3 present all important

geochemical information about pelitic granulite. The rare earth element pattern reveals a negative Eu anomaly together with a moderate LREE enrichment over the HREE (Fig. 6a), which indicates that the source of sediments has a likely composition similar to that of the upper crust. Compositions of the upper crust (UC), lower crust (LC) and bulk (BC) are plotted alongside sample data on spidergrams. All of the samples have a character that is comparable to the upper crust (the composition of the crust was taken from Taylor and McLennan, 1985). This also suggests that the source of sediments is upper crust composition. Pelitic granulite samples show similar trace element patterns in the primitive mantle-normalized trace element and spidergrams (Fig. 6b). These patterns are depleted in high field-strength

Table 3. Comparison of geochemical values of the pelitic granulite of study area

Sample No.	D/1	D/15	D/17	D/26	D/47	D/48	D/53	D/68	D/69	D/72	D/73	D/93
Al_2O_3/SiO_2	0.17	0.15	0.16	0.06	0.13	0.11	0.13	0.12	0.15	0.03	0.02	0.06
$Al_2O_3/(Na_2O + CaO)$	8.44	8.59	8.55	6.10	8.27	6.46	7.98	7.49	4.51	6.36	32.40	9.93
Al_2O_3/Na_2O	209.40	240.50	200.00	166.67	221.25	86.38	177.20	164.80	21.75	20.82	54.00	30.54
Al_2O_3/CaO	8.80	8.91	8.93	6.33	8.59	6.98	8.36	7.85	5.69	9.16	81.00	14.70
$Fe_2O_3 + MgO$	6.09	6.02	6.11	2.68	4.92	7.40	4.94	5.26	5.51	5.21	4.83	5.05
K_2O/Na_2O	3.00	3.00	2.80	1.67	2.75	1.00	2.40	2.00	0.33	0.18	1.67	0.38
K/Rb	18.16	18.08	16.99	12.25	19.17	18.62	15.68	17.09	23.98	19.97	10.82	19.87
La/Th	1.90	1.92	1.76	1.94	2.05	2.03	2.06	1.88	3.39	1.47	2.04	1.50
La/Sc	2.17	2.41	1.39	4.55	2.04	3.42	2.42	2.45	2.02	13.53	2.84	6.41
Th/Sc	1.14	1.25	0.79	2.35	1.00	1.68	1.17	1.30	0.59	9.18	1.39	4.26
Ni/Co	2.75	2.24	2.33	2.90	2.12	2.54	2.07	2.51	1.13	5.14	52.50	3.45
Sc/Ni	0.26	0.38	0.44	0.21	0.47	0.28	0.45	0.31	0.93	0.18	0.18	0.46
Sc/Cr	0.19	0.20	0.27	0.18	0.24	0.17	0.20	0.18	0.74	0.57	1.27	0.80
Ti/Zr	12.50	12.84	16.21	5.63	10.59	14.20	10.13	10.54	11.19	1.64	0.14	1.68
Zr/Th	2.16	1.84	1.94	3.50	2.45	1.78	2.57	2.67	7.54	2.45	11.94	2.48
Zr/Hf	36.87	36.72	36.58	36.05	37.04	36.32	37.76	37.76	40.44	34.57	22.93	34.28
La/Yb	12.49	13.18	5.75	18.58	9.25	22.48	9.98	11.92	8.11	76.67	1.05	29.68
Th/U	11.60	12.50	9.50	10.10	10.50	10.40	4.80	19.50	1.70	19.70	11.0	9.60
Eu/Eu*	0.168	0.167	0.165	0.167	0.166	0.169	0.167	0.168	0.164	0.168	0.170	0.169

elements (Nb, Ta and Ti) and enriched in large-ion lithophile elements (Rb, Th, U, K and Pb), suggesting that they are typical of continental crust composition. This observation is further supported with those of Biswal et al. 1998. However, the Sr, Nd and Pb compositions of the samples show large variations, which indicate two sources (felsic and mafic) of the sediments. The distribution of high field strength elements in the pelitic granulite, such as Zr, Hf, Nb and Ta, shows a wide range of possible values. Zr in the pelitic granulites that were analysed ranged from 40.60 ppm to 92.90 ppm, although the ratio of Zr to Hf stays rather stable between the values of 22.43 and 40.44. Ta fluctuates between 0.50 and 1.40 ppm. The fact is that the samples are deficient in Ta and Nb as well as Zr and Hf that give support to the hypothesis that Ta and Nb are bound up in zircon.

The pelitic granulites of ADMB are distinguished by their high concentrations of U and Th (Table 2b), in contrast to the moderate abundances of high field strength elements such as Zr and Y. The amount of uranium ranges from 1.60 to 3.10 ppm, while that of thorium ranges from 5.30 to 37.50 ppm. As a result, the samples that are currently analysed are distinguished by having different U and Th enrichment similar to that of Sen et al. (2009). An in-depth analysis of the Th/U ratio, which ranges from 1.70 to 19.70, reveals that there is a significantly greater abundance of Th than U in the pelitic granulites, which points to the presence of considerable thorium mineralization in the study area.

5.d. Implications on source rock characters

The ratio of Rb/Ba vs. Rb/Sr (Fig. 7) illustrates that the source of sediments is ancient rocks that are deficient in clay. It is worthwhile

to mention here that according to Taylor and McLennan (1985), the Archaean sedimentary rocks contain geochemical features that are noticeably distinct from those of the Proterozoic sedimentary rocks (Table 4), despite the fact that some overlaps are detected in certain locations (Naqvi et al. 1983: Gibbs et al. 1986; Smith et al. 1992; Raj & Naqvi, 1995). We recorded a compositional similarity with this area to Proterozoic sedimentary rocks, as shown in Table 4, a consistent strong negative Eu anomaly, a high K_2O value, low K/Rb and La/Th ratios, high La/Sc and Th/Sc ratios, very low Ni and Cr contents and uniform Zr/Hf ratio are suggestive of a Proterozoic age for the protolith (Wildeman & Haskin, 1973; Dypvik & Brunfelt, 1976: McLennan et al. 1980). According to Gyani (1995), similar to Archaean supracrustals, the granulites of the Banded Gneissic Complex have low levels of SiO_2 (58%), Th/U (3.5), high levels of MgO/Al_2O_3 (0.31) and low levels of Na_2O/Al_2O_3 (0.2) (Gyani, 1995), whereas present observation noticed higher values of the above ratios for the pelitic granulite (Tables 2a and 2c). In addition to the geochemical criteria, the deformational history of the pelitic granulite of the present study area contrasts with that of the Aravalli supergroup and the Banded Gneissic Complex, both of which demonstrate the earliest folding along an east-west axis (Naha et al. 1984; Roy, 1988), while the pelitic granulite, along with other components of the SDT, do not exhibit any evidence of folding (Biswal, 1988). Our geochemical observations and interpretation in conjunction with the geochronological data infer that granulites metamorphism in the research area is significantly younger than the granulites of the Archaean supracrustals and Banded Gneissic Complex.

Since the chemistry of sediments in each tectonic setting is distinct, it is determined by the mobility of various elements as
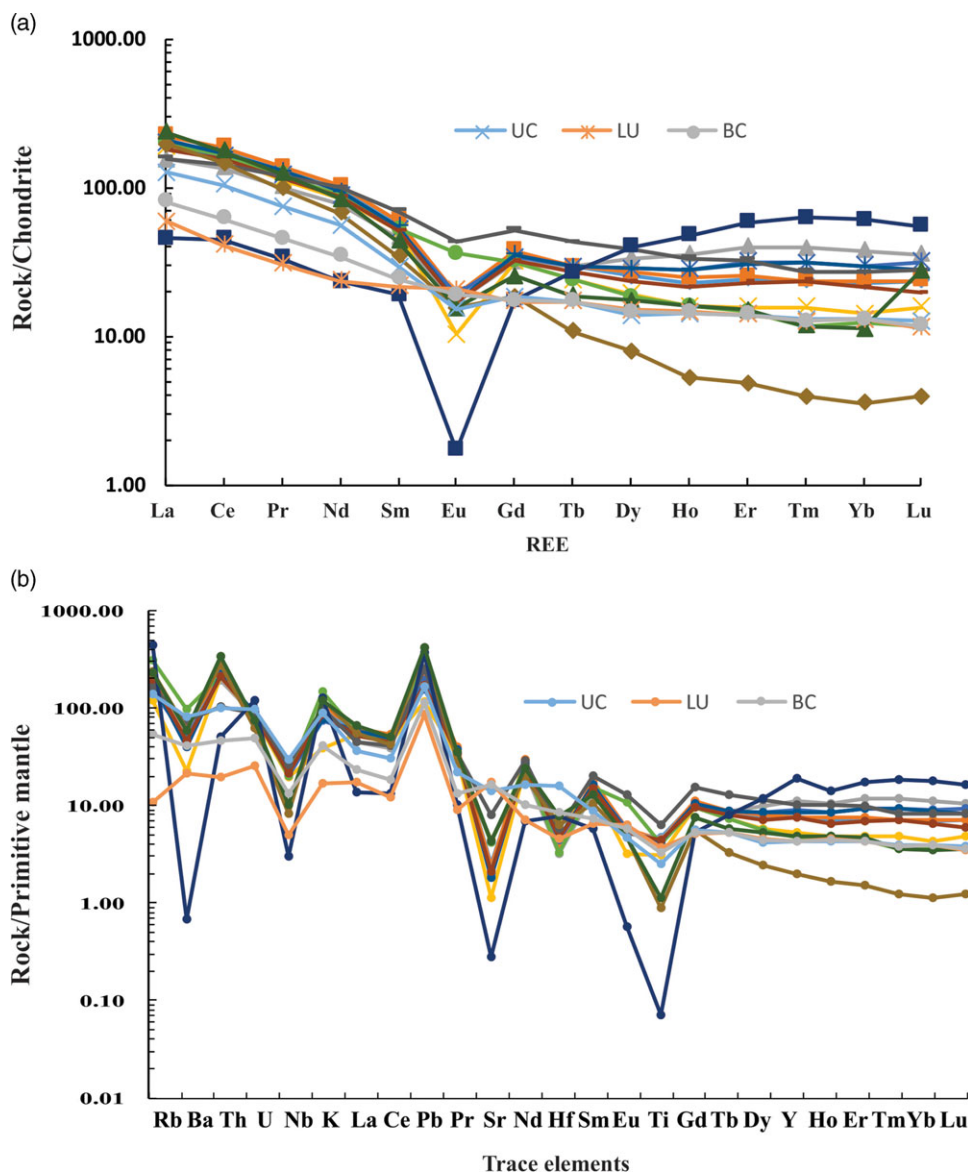
Figure 6. (Colour online) (a) Chondrite-normalized rare earth elements (REE) patterns in the pelitic granulites samples and (b) primitive mantle normalize trace elements spider diagram.

well as the recycling of sediments. The ratio of trace elements seen in the Th-Hf-Co (Fig. 8a) and La-Th-Sc (Fig. 8b) plots also provides support to the assumption that the probable tectonic environment might have been passive continental margins. The La/Sc, Ni/Co, Sc/Cr, La/Yb and K_2O/Na_2O geochemical values of the pelitic granulite of the study area also support our inference (Table 5).

6. Geochronology

6.a. Identification of monazite

Monazite is found in the rocks of the study area as an accessory phase. Since it is difficult to differentiate between monazite grains from zircon grains based only on their appearance, monazite grains were located by analysing BSE image in the present study (Fig. 9).
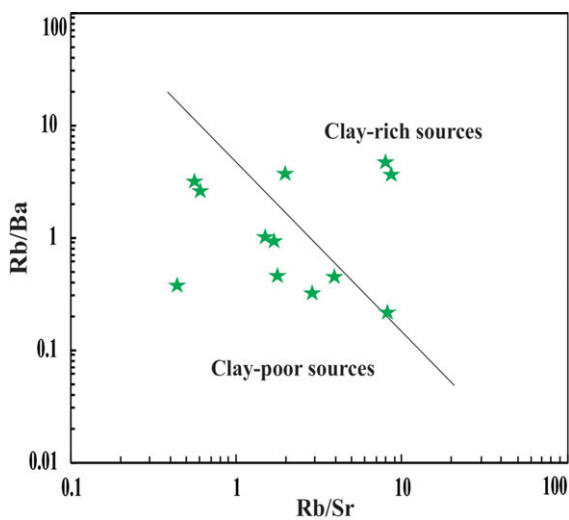
6.b. Monazite geochronology

The age of metamorphism and deformational history can be determined by means of electron microprobe analysed chemical dating, making it a useful tool in geological investigations (Williams 1999). In the DST-SERB National Facility at the Department of Geology (Center of Advanced Study) at the Institute of Science, Banasu Hindu University, Electron Probe Micro Analyzer (EPMA) CAMECA SXFive equipment was used to conduct the chemical dating. The BSE image marks the boundary of a homogeneous compositional region, as seen in the monazite grains (Fig. 9).

In this work, EPMA monazite geochronology was used to quantify the age of the pelitic granulite of SDT (ADMB) and to track the evolutionary history of the pelitic granulite. The mineral monazite is often found as an inclusion in garnet and other crystalline materials. We evaluate monazite growth events recorded at in the Diwani hill of ADMB and compare the ages

Table 4. Comparison of geochemical values of the pelitic granulite of the study area with rocks of different ages (McLennan *et al.* 1980, Taylorand McLennan, 1985)

	Av. Pelitic granulies	Proterozoic rocks	Archean rocks
Ni	44.08	<100	350.00
Cr	66.75	<150	600.00
K₂O	3.71	3.50	0.90
Rb	180.48	115.00	25.00
LREE/HREE	10.76	10.00	7.40
REE	99.77	146.40	70.30
REE pattern	Uniform	Uniform	Varible
La/Th	1.89	<2.8	>3.5
La/Sc	2.74	>2.7	<1.3
Th/Sc	1.44	>1.0	<0.43
K/Rb	170.75	250.00	>300
K/Na	3.18	>1.0	<1.0
Zr/Hf	Uniform	Uniform	Varible
La/Yb	10.43	10.00	3–9
MgO/Al₂O₃	0.14	0.14	0.24
CaO/Al₂O₃	0.13	0.12	0.22
Na₂O/Al₂O₃	0.02	0.12	0.19
K₂O/Al₂O₃	0.01	0.22	0.15

Table 5. Comparison of geochemical values of the pelitic granulite of the study area with rocks of different tectonic settings (Bhatia, 1983; Bhatia, 1985; Bhatia & Crook, 1986)

	OIA	CIA	ACM	PCM	D-H
Al₂O₃/SiO₂	0.29	0.20	0.18	0.10	0.21
Al₂O₃/CaO	1.72	2.42	2.56	4.15	29.14
Fe₂O₃ + MgO	11.73	6.79	4.63	2.89	9.10
K₂O/Na₂O	0.39	0.61	0.99	1.60	3.73
La/Sc	0.55	1.83	4.55	6.25	2.74
Th/Sc	0.15	0.85	2.59	3.06	1.44
Ni/Co	0.62	1.22	1.04	1.42	2.48
Sc/Ni	2.30	1.44	0.77	1.90	0.35
Sc/Cr	0.57	0.32	0.30	0.16	0.23
Ti/Zr	56.80	19.70	15.30	6.74	80.25
Zr/Th	48.00	21.50	9.50	19.10	2.77
La/Yb	2.80	7.50	8.50	10.80	10.43
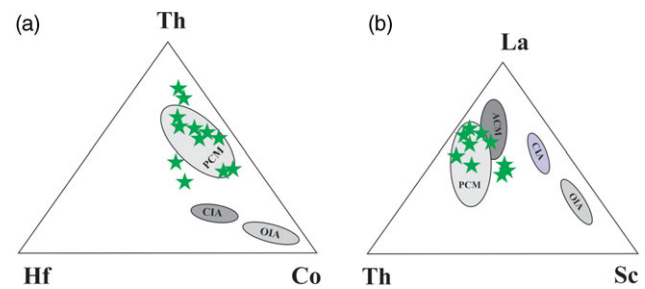
Figure 8. (Colour online) Differentiating the plate tectonic setting based on (a) Th, Hf and Co plotting and (b) La-Th-Sc to demonstrate the passive continental margin.

standard deviation of 0.26 Ma for detritus formed from a magmatic/sedimentary source for pelitic granulite, while Fig. 10b shows an age of 840.16 ± 8.08 Ma, with a mean standard deviation of 0.87 Ma for metamorphic thermal overprint. A density diagram of probabilities reveals two peaks (Fig. 10c).

7. Geodynamic evolution

The complete sequence of granulites development in this area, including the evolutionary tectonic history of ADMB, may be better revealed when these findings are paired with geochronological data. For this purpose, we have compared our present findings with some recent geochronological histories provided by previous workers (Bhowmik *et al.*. 2010; Singh *et al.* 2010, 2020; Tiwari & Biswal, 2019; Prakash *et al.* 2021; Biswal *et al.* 2022; Kumar *et al.* 2022; Tiwari *et al.* 2022). We have inferred, on the basis of our findings and geochronological interpretations that the collisional orogeny took place in the ADMB during the Grenvillian epoch (≈ca. 1090–980 Ma). In addition to this, discussion is held over the scale of the propagation of the Grenvillian orogenic front inside the Aravalli-Delhi orogen as well as its significance for the reconstruction of Rodinia supercontinent. According to Singh *et al.* (2010) explanation, the granulites are thought to have exposed through the action of thrusting along a number of ductile
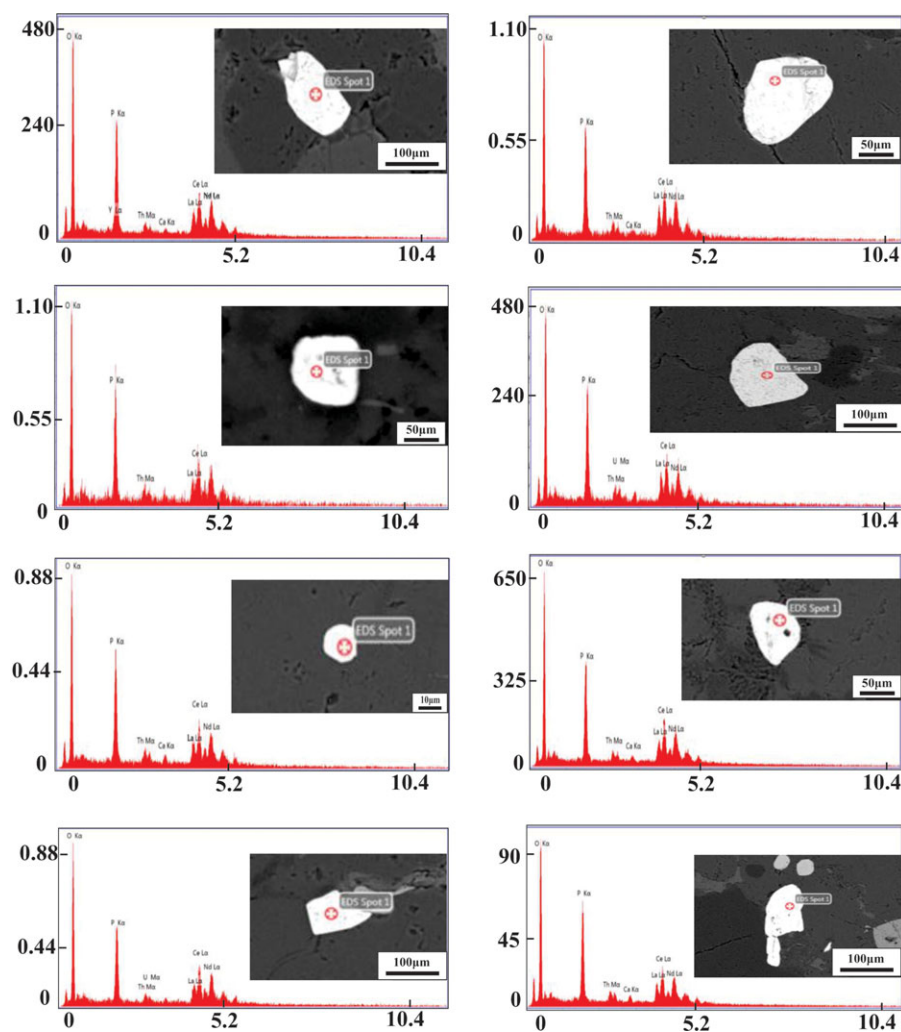

Figure 7. (Colour online) The composition of the protolith in the study area is depicted Rb/Ba vs Rb/Sr diagram, showing the source of sediments are deficient in clay.

and uncertainty of individual grains of monazite. Total 27 EPMA points have been analysed using two samples (D/52 and D/57) in several monazite grains (Table 6). The determined ages of monazites span the intervals of 1188 ± 56 to 1324 ± 25 Ma and 796 ± 40 to 906 ± 32 Ma, and Fig. 10 displays the weighted average age distribution and probability density plot. Figure 10a suggests a population age of 1213.8 ± 14.3 Ma, with a mean

Figure 9. (Colour online) Represents the backscattered images (BSE-SEM) of different monazite grains.

shear zones during the transition from syn- to post-F_2 folding (Bhowmik *et al.* 2010; Singh *et al.* 2010, 2020; Tiwari & Biswal, 2019; Biswal *et al.* 2022; Tiwari *et al.* 2022). The SHRIMP U-Pb chronology of zircons from pelitic granulite, according to Prakash *et al.* (2021), yields the ages between 780 Ma and 680 Ma as a period of metamorphic overprint, and the ages between 1591 Ma and 1216 Ma match well with detritus formed from a magmatic/ sedimentary source for pelitic granulite.

Based on previous work, it may be deduced that the depositional basin corresponds to passive continental margin (Biswal *et al.* 1998). This suggests that the Archaean BGC craton might have been rifted during the Proterozoic time, resulting in the formation of the basin at the trailing edge of a fragmented continental block. As per existing literature, palaeo-plate tectonic processes were responsible for the evolution of the Paleoproterozoic Aravalli and Mesoproterozoic Delhi fold belts of the Northwest Indian Shield (Singh *et al.* 2010, 2020; Tiwari & Biswal, 2019; Biswal *et al.* 2022; Tiwari *et al.* 2022). These belts were formed as a result of an accretionary process of island arcs, which occurred during subduction and/or collision. In the case of ADMB and SDT, the collision fabric that has been preserved are the island arc signal, the crustal scale imbricated thrust fault and the dipping reflectors all point to the formation of a thick

and stable crust during the Proterozoic epoch (Rao *et al.* 2000). The Proterozoic crustal thickness of the area corresponds well with the crustal thickness that has been measured across the entire planet (Rao *et al.* 2000). According to the findings of the present study, we inferred that the crust has not been appreciably changed since the Proterozoic collision, with the exception of re-equilibration occurring along the suture zones of the Aravalli and Delhi mountains. It leads us to infer that the Proterozoic crust was probably more stable having greater thickness than the Phanerozoic crust.

In the background of above discussion regarding mineral chemistry, petrography, geochemistry and geochronology, an attempt has been made to depict the numerous stages of evolution of the Aravalli-Delhi mobile Belts in the northwestern part of the Indian Shield (as suggested by Rao *et al.* 2000 and references therein) to ensure the compatibility of our findings. The geochemical analyses results suggest the existence of a proto-ocean in the region between Bundelkhand craton in the east and Marwar craton in the west (Bhowmik *et al.* 2010; Singh *et al.* 2010, 2020; Tiwari & Biswal, 2019; Biswal *et al.* 2022; Tiwari *et al.* 2022). Due to development of a compressional regime, the eastern craton migrated towards the west. Thus, the proto-oceanic crust together with sediments deposited on it subducted under Marwar craton.

Table 6. Analytical results from monazites of granulite using the EPMA U–Th–total Pb method

Points	SiO$_2$	P$_2$O$_5$	CaO	Y$_2$O$_3$	La$_2$O$_3$	Ce$_2$O$_3$	Pr$_2$O$_3$	Nd$_2$O$_3$	Sm$_2$O$_3$	Eu$_2$O$_3$	PbO	UO$_2$	ThO$_2$	Total	Age(Ma)	±2σ
D/70/15	0.18	29.96	1.48	0.72	16.51	29.23	4.17	8.57	0.96	0.35	0.20	0.61	7.11	102.88	1226	42
D/70/16	0.09	30.23	1.52	1.14	13.12	27.65	4.32	11.42	2.00	0.15	0.34	0.79	7.22	100.00	808	45
D/70/17	0.41	30.28	1.46	0.47	13.77	26.81	4.32	11.08	1.95	0.23	0.25	0.23	7.19	98.44	1308	39
D/70/18	0.24	31.24	1.45	0.24	13.90	28.52	4.32	11.98	2.27	0.02	0.27	0.45	6.00	100.89	846	54
D/70/19	0.34	30.38	1.31	0.16	14.02	28.68	4.53	12.35	2.20	0.03	0.27	0.14	4.57	98.99	1248	69
D/70/20	0.28	31.30	1.40	0.84	14.03	27.58	4.30	10.83	1.92	0.04	0.21	0.39	6.17	99.23	865	52
D/70/21	0.28	29.38	1.52	0.20	13.59	28.50	4.32	11.91	2.16	0.04	0.32	0.59	7.19	100.02	826	40
D/70/22	0.21	30.62	1.53	0.24	13.67	28.09	4.39	12.47	2.27	0.09	0.32	0.60	6.57	101.05	1255	44
D/70/23	0.23	31.07	1.19	0.12	14.19	29.33	4.59	12.40	2.27	0.06	0.24	0.47	5.16	101.31	843	62
D/70/24	0.25	30.87	1.01	0.20	14.19	29.42	4.82	12.59	2.43	0.07	0.24	0.43	4.13	100.66	906	32
D/70/25	0.23	30.60	1.71	0.46	13.22	27.52	4.49	11.82	2.16	0.07	0.32	1.25	6.56	100.36	876	37
D/70/26	0.15	29.91	1.51	1.10	13.02	27.21	4.32	11.47	2.03	0.01	0.30	1.04	5.84	97.88	828	28
D/52/27	0.31	27.38	1.32	0.30	13.84	28.47	4.76	11.99	1.97	0.04	0.22	0.22	6.76	97.60	1207	43
D/52/28	0.22	30.24	1.49	0.54	13.67	27.79	4.53	11.93	2.06	0.00	0.32	0.80	6.77	100.36	880	26
D/52/29	0.19	30.26	1.55	0.53	13.36	28.16	4.34	11.99	2.23	0.03	0.32	0.95	5.80	99.68	1324	25
D/52/30	0.19	30.58	1.58	0.49	13.60	29.02	4.29	11.81	2.11	0.01	0.35	1.14	6.31	101.47	808	34
D/52/31	0.19	30.31	1.34	0.51	13.58	28.06	4.52	12.00	2.18	0.00	0.30	0.86	5.86	99.70	1195	51
D/52/32	0.15	30.82	1.53	0.40	13.88	28.01	4.27	11.39	2.01	0.04	0.34	0.91	6.13	99.84	866	41
D/52/33	0.14	30.67	1.65	1.42	12.98	26.60	4.21	11.31	2.00	0.08	0.36	1.33	6.29	99.03	796	40
D/52/34	0.44	30.65	0.90	0.54	14.37	28.75	4.50	11.90	2.08	0.21	0.18	0.17	4.77	99.48	1188	56
D/52/35	0.44	29.44	1.35	0.72	13.12	28.48	4.45	12.25	2.11	0.01	0.23	0.15	6.58	99.33	809	35
D/52/36	0.17	31.43	1.47	0.65	13.30	28.25	4.48	12.16	2.06	0.05	0.24	0.28	5.83	100.31	824	33
D/52/37	0.25	30.13	1.46	0.46	13.21	27.40	4.39	11.73	2.06	0.05	0.34	0.96	6.83	99.23	801	44
D/52/38	0.36	29.57	1.58	0.57	12.78	26.81	4.10	11.66	2.08	0.00	0.38	1.30	6.45	97.65	1212	34
D/52/39	0.59	29.75	1.40	0.61	13.03	27.37	4.38	11.71	2.00	0.15	0.36	1.33	6.13	98.79	797	31
D/52/40	0.17	31.14	1.42	0.51	13.46	28.09	4.41	12.29	2.33	0.02	0.27	0.77	5.70	100.58	859	26
D/52/41	0.37	31.28	1.07	0.53	13.71	28.51	4.57	12.17	2.17	0.23	0.16	0.48	5.53	100.77	1216	34
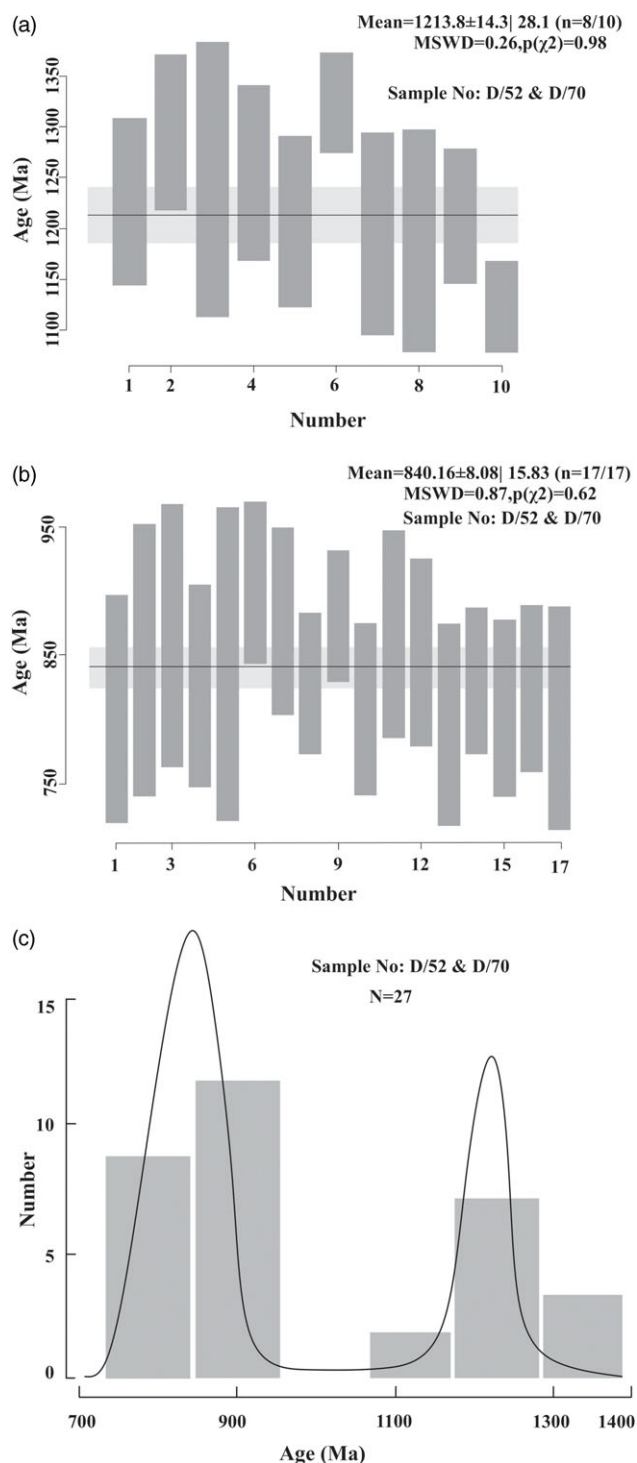
Figure 10. (Colour online) Displays the results of the ISOPLOT programme (Ludwig, 2011). (a) Weighted average older age distribution, (b) weighted average younger age distribution and (c) probability density plot.

Further convergence resulted in partial melting of ancient crustal rocks. As the collision continued, a crustal scale suture developed known as Aravalli Suture (Fig. 11a, b). Such kind of suturing at the subduction zone is a common phenomenon in many ancient collision boundaries of stable Precambrian regions. A condensed crust in such kind of subduction/collision zone usually provides

almost ideal pressure, temperature regime for the generation of granulites (Rao *et al.* 2000). According to Sinha-Roy *et al.* 1995, Sandmata granulites, which were thrusted up as tectonic wedges within the basement gneisses, generated under such an environment during Arawalli orogeny. In accordance with Rao *et al.* 2000 (and references theirin) following the evolution of the Paleoproterozoic Aravalli orogeny, during the Mesoproterozoic period, this region has undergone one more episode of rifting in the SDT. This might have resulted in the opening of an ocean between Bundelkhand-Aravalli-BGC craton and Marwar craton (Bhattacharya & Mukherjee, 1984) (Fig. 14c). The sediment deposited in this basin is regarded as Delhi sediments. This phase was followed by another compressional regime. As a result, western Marwar craton along with oceanic crust subducted eastward beneath the Bundelkhand-Aravalli-BGC craton (Fig. 11d). Due to the development of high pressure and low-temperature regime at the subduction zone, the blueschist facies metamorphism (Phulad ophiolites and related rocks) at the boundary of these colliding cratons took place. Furthermore, based on geochemical, geochronological and isotope studies, Volpe and Macdougall (1990) have reported that Phulad ophiolites and related rocks belong to fragments of the Proterozoic island arc complex. Our interpretation of geo-chemical and geochronological data suggests that during the probable diapiric rise, the magmatic material might have been contaminated due to the assimilation with the country crustal rocks. Consequently, the lithology became anhydrous, and successive metamorphic processes lead to the formation of granulites which later exhumed to the surface as a tectonic response.

8. Conclusion

According to mineral and elemental geochemistry analysis, and geochronological data, the pelitic granulite of the examined area suggest arkosic to shaly nature of the protolith. The REE pattern indicates that the source of sediments has a likely composition similar to that of the upper crust. However, the Sr, Nd and Pb indicate that two source (felsic and mafic) of sediments in varying proportions. Th-Hf-Co and La-Th-Sc provide support to the assumption that the probable tectonic environment might have been passive continental margins. Monazite geochronology dictates that the metamorphic overprint took place between 797 Ma and 906 Ma, and the ages that correspond to the debris was produced from magmatic/sedimentary sources for pelitic gran-ulites which lie between 1188 Ma and 1324 Ma. A deeper understanding of the Proterozoic era evolutionary history of the pelitic granulite that make up the SDT in the ADMB region is made possible by the current study.

Figure 11. (Colour online) Cartoon depicting different stages of evolution of the Aravalli-Delhi Fold Belts (ADMB) of the northwestern Indian Shield (after Rao *et al.* 2000).

References

Ahmad I and Mondal MEA (2016) Do the BGC-I and BGC-II domains of the Aravalli craton, northwestern India represent accreted terranes? *Earth Sciences India* **9**, 167–75.

Anbazhagan S, Biswal TK, Roy T, Kusuma KN, Banerjee DM and Bhattacharya P (2006) Remote sensing study of Petrology and geochemistry of greywackes from the Aravalli Supergroup, Rajasthan, India and the tectonic evolution of a Proterozoic sedimentary basin. *Precambrian Research* **67**, 11–35.

Bhatia MR (1983) Plate tectonics and geochemical composition of sandstones. *Journal of the Geological* **91**, 611–27.

Bhatia MR (1985) Rare earth element geochemistry of Australian Paleozoic graywackes and mudrocks: Provenance and Tectonic control. *Sedimentary Geology* **45**, 97–113.

Bhatia MR and Crook KA (1986) Trace element characteristics of graywackes and tectonic setting discrimination of sedimentary basins. *Contributions to Mineralogy and Petrology* **92**, 181–93.

Bhattacharya PK and Mukherjee AD (1984) Petrochemistry of metamorphosed pillow and the geochemical status of the amphibolites (Proterozoic) from the Sirohi district, Rajasthan India. *Geological Magazine* **121**, 465–73.

Bhowmik SK, Bernhardt HJ and Dasgupta S (2010) Grenvillian age high-pressure upper amphibolite-granulite metamorphism in the Aravalli-Delhi Mobile Belt, Northwestern India: new evidence from monazite chemical age and its implication. *Precambrian Research* **178**, 168–84.

Bhowmik SK and Dasgupta S (2012) Tectonothermal evolution of the Banded Gneissic Complex in central Rajasthan, NW India: present status and correlation. *Journal of Asian Earth Sciences* **49**, 339–48.

Bhowmik SK, Dasgupta S, Baruah S and Kalita D (2018) Thermal history of a Late Mesoproterozoic paired metamorphic belt (?) during Rodinia assembly: new insight from medium-pressure granulites from the Aravalli-Delhi Mobile Belt, Northwestern India. *Geoscience Frontiers* **9**, 335–54.

Biswal TK (1988) Polyphase deformation in Delhi rocks, southeast of Amirgad, Banaskantha district of Gujarat. *Memoir Journal of the Geological Society of India* **7**, 267–77.

Biswal TK, Gyani KC, Parthasarathy R and Pant DR (1998) Implications of the geochemistry of the Pelitic Granulites of the Delhi Supergroup, Aravalli Mountain Belt, Northwestern India. *Precambrian Research* **87**, 75–85.

Biswal TK, Gyani KC, Parthasarathy R and Pant DR (1998a) Tectonic implication of geochemistry of gabbro-norite-basic granulite suite in the Proterozoic Delhi Supergroup, Rajasthan. India. *Journal of the Geological Society of India* **52**, 721–32.

Biswal TK, Pradhan RM, Sharma NK, Tiwari SK, Beniest A, Behera BM, Singh S, Saraswati R, Bharadwaj A, Umasankar BH, Singh YK, Sarkar S, Mahadani T and Saha G (2022). A review on deformation structures of different terranes in the Precambrian Aravalli-Delhi Mobile Belt (ADMB), NW India: tectonic implications and global correlation. *Earth-Science Reviews* **230**, 104037.

Biswal TK, Sarkar S, Pal A and Chakaraborty U (2004) Pseudotachylites of the KuiChitraseni shear zones of the Precambrian Aravalli Mountain, Rajasthan. *Journal of the Geological Society of India* **64**, 325–35.

Choudhary AK, Gopalan K and Sastry CA (1984) Present status of the geochronology of the Precambrian rocks of Rajasthan. *Tectonophysics* **105**, 131–40.

Crawford AR (1970) The Precambrian geochronology of Rajasthan and Bundelkhand, northern India. *Canadian Journal of Earth Sciences* **7**, 91–110.

D'Souza J, Prabhakar N, Sheth H and Xu Y (2021) Metamorphic P-T-t-d evolution of the Mesoproterozoic Pur-Banera supracrustal belt, Aravalli Craton, northwestern India: insights from phase equilibria modelling and zircon-monazite geochronology of metapelites. *Journal of Metamorphic Geology* **39**, 1173–204.

Deb M and Thorpe RI (2001) Geochronological constraints in the Precambrian Geology of Northwestern India and their Metallogenic Implication. In *Pre-Seminar Volume on International Workshop on Sediment-hosted LeadZinc Sulfde Deposit in the Northwestern Indian Shield, Delhi-Udaipur, India* (eds M Deb and WD Goodfellow), pp. 137–52. New Delhi: Prepared at Department of Geology, Delhi University.

Deb M, Thorpe RI, Krstic D, Corfu F and Davis DW (2001) Zircon U-Pb and galena Pb isotope evidence for an approximate 1.0 Ga terrane constituting the western margin of the Aravalli–Delhi orogenic belt, northwestern India. *Precambrian Research* **108**, 195–213.

Desai SJ, Patel MP and Merh SS (1978) Polymetamorphites of Balaram-Abu Road area, north Gujarat and southwestern Rajasthan. *Journal of the Geological Society of India* **19**, 383–94.

Dypvik H and Brunfelt AO (1976) Rare-earth elements in Lower Palaeozoic epicontinental and eugeosynclinal sediments from the Oslo and Trondheim regions. *Sedimentology* **23**, 363–78.

Fareeduddin KA (1998) Single zircon age constraints on the evolution of Rajasthan granulite. In *The Indian Precambrian* (ed BS Paliwal), pp. 547–56. Jodhpur: Scientfc Publishers India.

Gibbs AK, Montgomery CW, O'Day PA, Erslev EA (1986) The Archean-Proterozoic transition: evidence from the geochemistry of metasedimentary rocks of Guyana and Montana. *Geochemical and Cosmochemical Journal* **50**, 2125–41.

Gyani KC (1995) Granulites from Bhinai-Bandanwara region, Ajmer district. Rajasthan. Western India: petrochemistry, fluid inclusions and P-T conditions. In *Proceeding National Seminar on Recent Research in Geology of West India* (eds N Desai and S Ganapati), pp. 241–66. Vadodara: University of Baroda.

Heron AM (1553) The geology of central Rajputana. *Memoir Geological Survey of India* **79**, 389.

Kumar A, Prakash A, Saha L, Corfu F and Bhattacharya A (2019) 940 Ma anatexis in 1726 Ma orthogneiss in the northern margin of the Bhilwara belt and significance for the precambrian evolution in northwest India. *Journal of Geological* **127**, 627–41.

Kumar M, Prakash D, Singh CK, Yadav MK, Tewari S, Singh PK and Mahanta B (2022) Geochronology and oxygen fugacity of the pelitic granulite from the Diwani hills, NE Gujarat (NW India). *Geological Magazine* **160**, 22–34.

Ludwig KR (2011) *Isoplot 3.70 (version-4): A Geochronological Toolkit for Microsoft Excel.*, Berkeley, CA: Berkeley Chronology Center, Special Publication 4.

McLennan SC, Nance WB and Taylor SR (1980) Rare earth element thorium correlations in sedimentary rocks and the composition of the continental crust. *Geochimica et Cosmochimica Acta* **44**, 1833–9.

Mukhopadhyay D, Chattopadhyay N and Bhattacharyya T (2010) Structural evolution of a gneiss dome in the axial zone of the Proterozoic South Delhi Fold Belt in Central Rajasthan. *Journal of the Geological Society of India* **75**, 18–31.

Naha K and Halyburton RV (1974) Early Precambrian stratigraphy of central and southern Rajasthan, India. *Precambrian Research* **1**, 55–73.

Naha K, Mukhopadhyay DK, Mohanty R, Mitra SK and Biswal TK (1984) Significance of contrast in the early stages of the structural history of the Delhi and the pre-Delhi rock groups in the Proterozoic of Rajasthan, western India. *Tectonophysics* **105**, 193–206.

Naqvi SM, Condie KC and Allen P (1983) Geochemistry of some unusual early Archaean sediments from Dharwar craton, India. *Precambrian Research* **22**, 125–47.

Pandit MK, Carter LM, Ashwal LD, Tucker RD, Torsvik TH, Jamtveit B and Bhushan SK (2003) Age, petrogenesis and signifcance of 1 Ga granitoids and related rocks from the Sendra area, Aravalli Craton, NW India. *Journal of Asian Earth Sciences* **22**, 363–81.

Pownall JM, Hall R, Armstrong RA and Forster MA (2014) Earth's youngest known ultrahigh-temperature granulites discovered on Seram, eastern Indonesia. *Geology* **42**, 279–82.

Prakash D, Kumar M, Rai SK, Singh CK, Singh S, Yadav R, Jaiswal S, Srivastava V, Yadav MK, Bhattacharjee S and Singh PK (2021) Metamorphic P-T evolution of Hercynite-quartz-bearing granulites from the Diwani hills, North East Gujarat (NW India). *Precambrian Research* **352**, 105997.

Raj BU and Naqvi SM (1995) Relicts of sedimentary precursors in archean gneisses-melukote paragneiss-an example from Dharwar Craton, India. *Journal of the Geological Society of India* **46**, 497–520.

Rao VV, Prasad BR, Reddy PR and Tewari HC (2000) Evolution of Proterozoic Aravalli Delhi fold belt in the northwestern Indian shield from seismic studies. *Tectonophysics* **327**, 109–30.

Roy AB, Dutt K and Rathore S (2016) Development of ductile shear zones during diapiric magmatism of nepheline syenite and exhumation of granulites–examples from central Rajasthan, India. *Current Science* **110**, 1094–101.

Roy AB, Kröner A, Rathore S, Laul V and Purohit R (2012) Tectono-metamorphic and geochronologic studies from Sandmata complex, north-west Indian shield: implications on exhumation of late-palaeoproterozoic granulites in an archaean-early palaeoproterozoic granite-gneiss terrane. *Journal of the Geological Society of India* **79**, 323–34.

Roy AB (1988) Stratigraphic and tectonic framework of the Aravalli Mountain Range. In *Precambrian of the Aravalli Mountain* (ed AB Roy), pp. 33–75. Rajasthan, India: Memoir Geological Society of India.

Sarkar G, Burman TR and Corfu F (1989) Timing of continental arc-type magmatism in northwest India: evidence from U-Pb zircon geochronology. *Journal of Geological* **97**, 607–12.

Sarkar S and Biswal TK (2005) Tectonic significance of fissure veins associated with pseudotachylites of the Kui-Chitraseni Shear Zone, Aravalli Mountain, NW India. *Gondwana Research* **8**, 277–82.

Sen J, Ranganath N, Rathaiah YV, Sen DB and Kak SN (2009) Petrography and geochemistry of uranium mineralised Precambrian granitic-pegmatitic rocks of Mawlait, West Khasi Hills district, Meghalaya. *Journal of the Geological Society of India* **74**, 639–45.

Sen S (1980) Precambrian stratigraphic sequence in a part of the Aravalli range, Rajasthan: re-evaluation. *Quarterly journal of the Geological, Mining, and Metallurgical Society of India* **43**, 181–211.

Singh S, Shukla A, Umasankar BH and Biswal TK (2020) Timing of South Delhi orogeny: interpretation from structural fabric and granite Geochronology, Beawar-RupnagarBabra area, Rajasthan, NW India. In *Structural Geometry of Mobile Belts of the Indian Subcontinent, Society of Earth Scientists Series* (ed TK Biswal, *et al.*), pp. 1–22. Switzerland AG: Springer Nature.

Singh YK, De Waele B, Karmakar S, Sarkar S and Biswal TK (2010) Tectonic setting of the Balaram-Kui-Surpagla-Kengora granulites of the South Delhi Terrane of the Aravalli Mobile Belt, NW India and its implication on correlation with the East African Orogen in the Gondwana assembly. *Precambrian Research* **183**, 669–88.

Sinha-Roy S, Malhotra G and Guha DB (1995) A transect across Rajasthan Precambrian terrain in relation to geology, tectonics and crustal evolution of south-central Rajasthan. *Memoir Geological Survey of India* **31**, 63–89.

Smith MS, Dymek RF and Chadwick B (1992) Petrogenesis of Archaean Malene supracrustal rocks, NW Buksefjorden region, West Greenland: geochemical evidence for highly evolved Archaean crust. *Precambrian Research* **57**, 49–90.

Srikarni C, Limaye MA and Janardhan AS (2004) Sapphirine-bearing Granulites from Abu-Balaram Area, Gujarat State: implications for India-Madagascar Connection. *Gondwana Research* **7**, 1214–8.

Srivastava DC (2001) Deformation pattern in the Precambrian basement around Masuda, central Rajasthan. *Journal of the Geological Society of India* **57**, 197–222.

Sugden TJ, Deb M and Windley BF (1990) The tectonic setting of mineralisation in the Proterozoic Aravalli-Delhi orogenic belt, NW India. In *Precambrian Continental Crust and Its Economic Resources* (ed SM Naqvi), pp. 367–90. New York: Elsevier.

Taylor SR and McLennan SM (1985) *The Continental Crust: Its Composition and Evolution*. Oxford: Blackwell, p. 312.

Tiwari SK, Beniest A, Rai P, Chatterjee S, Daphale RV, Biswal TK, Yadav AK and Kundu S (2022) Implication of dynamic recrystallization mechanism for the exhumation of lower crustal rocks: a case study in the Shear Zones of the Ambaji Granulite, NW India. *Lithosphere* **2021**(Special 6), 6593243.

Tiwari SK and Biswal TK (2019) Dynamics, EPMA Th-U-Total Pb monazite geochronology and tectonic implications of deformational fabric in the lower-middle crustal rocks: a case study of Ambaji Granulite, NW India. *Tectonics* **38**, 2232–54.

Tobisch OT, Collerson KD, Bhattacharya T and Mukhopadhyay D (1994) Structural relationship and Sm–Nd isotope systematics of polymetamorphic granitic gneisses and granitic rocks from central Rajasthan, India-implications for the evolution of the Aravalli craton. *Precambrian Research* **65**, 313–39.

Volpe AM and Macdougall JD (1990) Geochemistry and isotopic characteristics of mafic (Phulad Ophiolite) and related rocks in the Delhi Supergroup, Rajasthan, India: implications for rifting in the Proterozoic. *Precambrian Research* **48**, 167–91.

Wildeman TR and Haskin LA (1973) Rare earths in Precambrian sediments. *Geochemical and Cosmochemical Journal* **37**, 419–38.

Williams PJ (1999) Metalliferous economic geology of the Mt Isa eastern succession. *Queensland Australian Journal of Earth Sciences* **45**, 329–341.